

Relationship between psychophysical measures of retinal ganglion cell density and *in vivo* measures of cone density in glaucoma

J Matlach, MD^{1,5}, PJ Mulholland, PhD^{1,2}, M Cilkova, MSc¹, R Chopra, BSc¹, N Shah, BSc¹, T Redmond, PhD³, SC Dakin, PhD⁴, DF Garway-Heath, MD FRCOphth¹, RS Anderson, DSc^{1,2}

¹NIHR Biomedical Research Centre, Moorfields Eye Hospital & UCL Institute of Ophthalmology, London, United Kingdom.

²Vision Science Research Group, Ulster University, Coleraine, United Kingdom.

³School of Optometry and Vision Sciences, Cardiff University, Cardiff, United Kingdom.

⁴Department of Optometry & Vision Science, University of Auckland, Auckland, New Zealand.

⁵Department of Ophthalmology, University Medical Center, Johannes Gutenberg University Mainz, Germany.

Results were presented at the ARVO meeting, 3rd – 7th May 2015, Denver, USA.

Financial Support

Supported by Dr Hans and Mrs Gertrude Hirsch award from Fight for Sight UK to Tony Redmond and Roger S Anderson. Juliane Matlach received funding from Dr. Werner Jackstädt-Stiftung. Pádraig J Mulholland receives support from the College of Optometrists (UK), in the form of a Clinical Research Fellowship. David Garway-Heath is funded in part by the National Institute for Health Research (NIHR) Biomedical Research Centre based at Moorfields Eye Hospital and UCL Institute of Ophthalmology. David Garway-Heath's chair at UCL is supported by funding from the International Glaucoma Association. The sponsors or funding organizations named above had no role in the design or conduct of this research. The views expressed are those of the author(s) and not necessarily those of the NHS, the National Institute for Health Research, or the Department of Health.

Conflict of interest

Juliane Matlach: None

Pádraig J Mulholland: Heidelberg Engineering (travel support)

Marketa Cilkova: None

Reena Chopra: None

Nilpa Shah: None

Tony Redmond: Heidelberg Engineering (research support)

David F Garway-Heath: Heidelberg Engineering (research support, speaker's fees), Carl Zeiss Meditec (research support), Topcon (research support), OptoVue (research support)

Roger S Anderson: Heidelberg Engineering (research support)

The sponsor or funding organization had no role in the design or conduct of this research.

Address for reprints

Roger Anderson, DSc, Vision Science Research Group, Ulster University, Coleraine, BT52 1SA, United Kingdom.

Email: rs.anderson@ulster.ac.uk

Abbreviations and Acronyms

AO, adaptive optics; AUROC, area under the receiver operator characteristic; CI, confidence interval; CRS, Cambridge Research Systems; CRT, Cathode Ray Tube; DLS, differential light sensitivity; DS, diopter sphere; DC, dioptre cylinder; GC, ganglion cell; GCL, ganglion cell layer; HFA, Humphrey Field Analyzer; HRA2, Heidelberg Retina Angiograph 2; HRT, Heidelberg Retina Tomograph; IEC, International Electrotechnical Commission; IOP, intraocular pressure; IPT, image processing toolbox; IQR, interquartile range; MAR, minimum angle of resolution; MD, mean deviation; OCT, optical coherence tomography; PGRA, peripheral grating resolution acuity; PSD, pattern standard deviation; RNFL, retinal nerve fibre layer; ROC, receiver operator characteristic; SAP, standard automated perimetry; SITA, Swedish Interactive Threshold Algorithm; VA, visual acuity

ABSTRACT

Purpose

There is considerable between subject variation in retinal ganglion cell (GC) density in healthy individuals, making identification of change from normal to glaucoma difficult. Ascertaining local cone:GC density ratios in healthy individuals, we wished to investigate the utility of objective cone density estimates as a surrogate of baseline GC density in glaucoma patients, and thus a more efficient way of identifying early changes.

Design

Exploratory cohort study.

Participants

Twenty glaucoma patients (60% female) with a median age of 54 years and mean deviation (MD) in the visual field (VF) of -5 dB and 20 healthy controls (70% female) with a median age of 57 years and MD of 0 dB were included.

Methods

Glaucoma patients and healthy subjects underwent *in vivo* cone imaging at 4 locations of 8.8° eccentricity with a modified Heidelberg Retina Angiograph HRA2 (scan angle of 3°). Cones were counted using an automated programme. GC density was estimated at the same test locations from peripheral grating resolution acuity (PGRA) thresholds.

Main Outcome Measures

Retinal cone density, estimated GC density and cone:GC ratios in glaucoma patients and healthy controls.

Results

Median [interquartile range, IQR] cone:GC density was 3.51:1 [2.59:1, 6.81:1] in glaucoma patients compared to 2.35:1 [1.83:1, 2.82:1] in healthy subjects . GC density was 33% lower in glaucoma patients than in healthy subjects, however cone density was very similar in glaucoma patients (7,248 cells/mm²) and healthy controls (7,242 cells/mm²).The area under the receiver operator characteristic curve was 0.79 (95% confidence interval [CI] 0.71-0.86, $P<0.001$) for both GC density and cone:GC ratio, and 0.49 (95% CI 0.39-0.58, $P=0.79$) for cone density.

Conclusions

Local measurements of cone density do not differ significantly from normal in glaucoma patients despite large differences in GC density. There was no statistically significant association between GC density and cone density in the normal participants, and the range of cone:GC density ratios was relatively large in healthy controls. These findings suggest that estimates of baseline GC density from cone density are unlikely to be precise, and offer little advantage over determination of GC alone in the identification of early glaucomatous change.

Key words

Retinal cone mosaic, glaucoma, ganglion cell density, psychophysics, cone imaging, Heidelberg Retina Angiograph

Introduction

Between-individual variability in retinal ganglion cell (GC) density in healthy human eyes is known to be high.¹ As a result, when a patient suspected of having glaucoma presents for the first time, it is difficult to determine whether a clinical measurement relating to GC density (e.g., conventional perimetry, peripheral grating resolution acuity [PGRA], or imaging parameter) is normal for the individual or already represents a change from that individual's original baseline. If, however: a) the cone:GC ratio is relatively similar between normal individuals (despite large inter-individual variation in both cone and GC density), and b) the number of cones remains stable in glaucoma (despite a decline in GC density), then objective cone density measures could be used as a means to determine the original baseline GC density and thus help to identify early GC loss in glaucoma without a lengthy longitudinal investigation.

While the death of retinal GC is a hallmark of glaucoma, the notion of a loss of cones in glaucoma is somewhat controversial. A loss of cones has been reported in several studies²⁻⁵, but this has not been confirmed in other studies.^{6, 7} With the introduction and development of adaptive optics (AO) technology, *in vivo* imaging of retinal structures at cellular level has become possible.⁸ More recently, Wolsley *et al* demonstrated that, by narrowing the scan width of the Heidelberg Retina Tomograph (HRT), the parafoveal photoreceptor mosaic may be imaged *in vivo* with a commercially available clinical device, without the need for AO.⁹ Similarly, images of the retinal cones can also be obtained *in vivo* using a modified Heidelberg Retina Angiograph 2 (HRA2), in a patient-friendly clinical setting.

In this study we used measurements of PGRA¹⁰ to estimate GC density at various locations outside the fovea. We also used a modified, small-angle HRA2 to image retinal cones *in vivo* at the same locations. By separately measuring cone and GC density at identical locations in both healthy subjects and glaucoma patients we

wished to a) explore the possibility of estimating what was the local baseline GC density in glaucoma patients from *in vivo* measurements of cone density using normal cone:GC density ratios , b) establish between-individual variability in cone:GC density in healthy observers, and c) investigate the utility of cone:GC density ratios in the identification of glaucoma.

Methods

Participants

The study protocol was approved by both the relevant National Health Service Research Ethics Committee and the UCL Research Ethics Committee. The research followed the tenets of the Declaration of Helsinki and written informed consent was obtained from all participants prior to inclusion.

Twenty open-angle glaucoma patients with a median age of 54 years and mild to moderate, mainly localized, visual field loss (median [IQR]: mean deviation (MD), -5 dB [-9, -4]; pattern standard deviation (PSD), 8 dB [6, 10]), and 20 age-similar healthy controls with a median age of 57 years underwent *in vivo* cone imaging with a HRA2 in addition to co-localized estimates of PGRA and differential light sensitivity (DLS). Inclusion criteria for glaucoma patients were: a diagnosis of open-angle glaucoma (including normal tension glaucoma), 'outside normal limits' readings for optic disc imaging according to Moorfields Regression Analysis using Heidelberg Retina Tomograph (HRTII; Heidelberg Engineering GmbH, Heidelberg, Germany) and overall or focal loss of peripapillary retinal nerve fibre layer (RNFL) in optical coherence tomography imaging (Spectralis OCT, Heidelberg Engineering GmbH, Heidelberg, Germany), in addition to a confirmed glaucomatous visual field defect as determined by standard automated perimetry (SAP) with the Humphrey Field Analyzer (HFAII; Carl Zeiss Meditec, Dublin, CA) 24-2 Swedish Interactive Threshold Algorithm (SITA)

strategy. A glaucomatous visual field defect was defined as a reduction in sensitivity at two or more contiguous locations with $P < 0.01$ loss or more, three or more contiguous points with $P < 0.05$ loss or more.¹¹ Inclusion criteria for healthy subjects were 'within normal limits' results for optic disc imaging (HRTII and OCT) and a full visual field. Subjects with a reliable visual field with fewer than 30% fixation losses and less than a 15% false-positive rate were included. All subjects had intraocular pressure (IOP) < 21 mmHg, refractive error < 6.00 DS and < 1.50 DC, and visual acuity (VA) of 20/30 (6/9) or better in the test eye, in the absence of significant corneal or media opacities. Exclusion criteria were the evidence of any systemic disease or medication which affects visual performance (e.g. diabetes, thyroid disease), any ocular disease (other than glaucoma for the glaucoma group), and surgery that may affect visual performance (e.g. resulting in poor visual acuity, refractive error outside above stated range).

After completion of preliminary tests, *in vivo* cone imaging with a modified small-angle HRA2, localized measurements of DLS and PGRA to estimate GC density, and thickness measurement of the ganglion cell layer (GCL) were performed as described below. One experienced operator (JM) performed all tests. If both eyes met inclusion and exclusion criteria in glaucoma patients and normal controls, the right eye was chosen.

Psychophysical tests

Peripheral Grating Resolution Acuity (PGRA)

PGRA was measured in the corresponding visual field locations with achromatic Gabor patches in sine phase (SD x Spatial frequency: 4; Michelson contrast: 99%; mean luminance: 30 cd/m²), presented on a uniform 30 cd/m² grey background varying in spatial frequency. Experiments were undertaken on a gamma-corrected Phillips FIMI

MGD-403 Achromatic CRT monitor (Ampronix, Irvine, CA, USA; refresh rate: 80 Hz, pixel resolution: 976 x 1028), driven by a Visual Stimulus Generator (ViSaGe MKII, Cambridge Research Systems, Rochester, UK) and the Cambridge Research Systems (CRS) toolbox (version 1.27) for MATLAB (R2014b, The MathWorks Inc., Natick, MA). Responses were collected using a Cedrus RB-530 response box (Cedrus Corporation, San Pedro, CA, USA). Participants were asked to view a cross-hair fixation target on the CRT monitor at a viewing distance of 60 cm and report whether the grating, presented at 8.8° eccentricity along the 45°, 135°, 225° and 315° meridians for 500 ms, was orientated either horizontally (180°) or vertically (90°). Resolution acuity was determined using a 3/1 reversal strategy, taking the average of four reversals, where the first two reversals resulted in a spatial frequency change of 20%, the third reversal a 10% change and the final reversal 5% change. Gabor patches scaled in size to maintain a constant number of high contrast cycles within the patch at all times to optimize resolution performance.¹² All subjects were optically corrected for the test distance and the eye not being tested was occluded. Resolution acuity values were then converted from minimum angle of resolution (MAR) to GC density (D, in GC/mm²) using the equation $MAR = 0.93/\sqrt{D}$ for a hexagonal array.¹³ A conversion factor from Drasdo & Fowler¹⁴ was used to calculate the number of GCs per square millimeter of the retina.

Differential light sensitivity (DLS)

Contrast thresholds were measured for an approximate Goldmann III size achromatic stimulus (0.48°, 0.18 deg²) of duration¹⁵ 191.9 ms at the same visual field locations (8.8° eccentricity along the 45°, 135°, 225° and 315° meridians). Stimuli were generated with a ViSaGe MKII and the CRS toolbox for MATLAB. Participants were instructed to view the central fixation target and press a button on a response pad

(Cedrus RB-530) when a stimulus was seen. A randomly interleaved 1/1 staircase (step size 0.5 dB of the previous value) terminating after six reversals was used, with threshold contrast being calculated as the mean of the final four reversals. Contrast thresholds were expressed in Humphrey equivalent dB values.

***In vivo* cone imaging using a modified small-angle HRA2**

A standard HRA2 (Heidelberg Engineering GmbH, Heidelberg, Germany) was modified for high resolution imaging of the fundus. For this purpose the scan angle was reduced by a factor of 10x to image fields of view of 3°, 2° and 1.5°, while the total number of pixels remained unchanged. This resulted in an oversampling of the diffraction limited spot size with the cone mosaic becoming visible (Fig 1 A, B). The images were acquired using a diode laser emitting at 815 nm working under reflection mode. The laser power was confirmed to be safe without restrictions, according to International Electrotechnical Commission (IEC) 60825-1:2007. To assess different areas of the fundus, the internal fixation lights could be adjusted manually by means of externally accessible alignment tools. *In vivo* imaging of the retinal cone mosaic was performed at four retinal locations (inferior nasal, inferior temporal, superior nasal, superior temporal retina) at 8.8° eccentricity along the 45°, 135°, 225° and 315° retinal meridians, through undilated pupils with room lights on (Fig 1 C, D). Subjects were instructed to look at the center of one of the cross-hair fixation targets, positioned at one of four pre-determined locations relative to the scan window, to enable imaging at the desired locations. Single, non-averaged *en face* reflectance images were collected and analyzed. The field of imaging was 3° × 3°, equating to 0.825 x 0.825 mm on the retina, based on Drasdo and Fowler's conversion for the relevant retinal location.¹⁴

Image analysis

Raw images of the cone mosaic ($\sim 3^\circ \times 3^\circ$, 768 x 768 pixels) were initially cropped to remove any extraneous features (e.g., scale bar, company logo, etc.). Cones were then identified in the cropped image ($\sim 2.89^\circ \times 2.89^\circ$, 740 x 740 pixels) by the method of Li & Roorda¹⁶, in MATLAB (R2014b) with the image processing toolbox (IPT). Briefly, this analysis first applies a low-pass filter in the frequency domain to the image to remove high-frequency noise from the image. Following this, the image is converted back to the spatial domain and the local luminance maxima detected using the IPT function *imregionalmax*. These identified regions were assumed to be cone centers and were plotted as single white pixels on a black background. To ensure the identified cones were not closer than physiologically possible, the binary blobs were each dilated using a white disk of diameter 2 pixels (i.e., if inter-cone spacing were too small, the given identified cones would no longer be spatially independent following dilation). Following this, each remaining spatially independent blob was counted as a cone. This value was then converted to a density value expressed as cones/mm². This method has been shown to provide cone density estimates that are very similar to those determined through manual counts, with the spatial localization of identified cones also being accurate for images acquired with AO technology.¹⁶ Figure 2 shows an example of the worst, typical and best quality image we captured in our participants and the automated cone count of the scan with the best quality.

Ganglion cell layer thickness

Automated segmentation and thickness measurement of the GCL was performed on the posterior pole scans (Spectralis OCT, acquisition software version 5.7.4.0). The grids on the posterior pole GCL thickness scans were rotated and translated to align with individual cone images (squares of grid also $3^\circ \times 3^\circ$, Fig 3).

Statistical analysis

Statistical analyses were performed with SPSS 23 (IBM Corporation, Armonk, NY, USA) and R (version 3.0.0, The R project). Median [interquartile range, IQR] GC and cone densities (cells/mm²), and cone:GC ratios, were calculated for glaucoma patients, and compared with those in age-similar healthy controls. A Mann-Whitney *U* test was used to test for statistically significant differences between groups and Friedman's two-way analysis of variance between locations within groups. Linear regression analysis was used to investigate the relationship between cone and GC density, cone:GC ratio and GCL thickness (from OCT) to corresponding DLS values (expressed in Humphrey equivalent dB values). Cone and GC density and GCL thickness were converted to log values for comparison with DLS. Receiver operator characteristic (ROC) curves and associated area under the receiver operator characteristic curve (AUROC) values were used to compare cone:GC ratio, GC density and cone density for diagnostic accuracy in the detection of glaucoma. Sixty-nine of 80 locations in glaucoma patients and 75 of 80 locations in healthy controls were included in the analysis. Scans where no cones could be resolved by eye were excluded from analysis. Glaucoma was seen as the positive test result. The ROC curves were used to estimate the sensitivity of GC density and cone:GC ratio at set specificities of 80% and 90%. For all analyses listed, a *P* value of <0.05 was considered statistically significant. To avoid type I errors we performed a Holm-Bonferroni correction where a) there were multiple tests of the same hypothesis (e.g. testing statistical significance of differences between data in superior and inferior hemifields) and b) p-values for individual tests are less than 0.05.

Results

General characteristics of glaucoma patients and age-similar healthy controls are given in Table 1. There was no statistically significant difference between each group in terms of age, gender, visual acuity, spherical refractive error or IOP (all $P > 0.05$).

GC density, cone density and cone:GC ratio

Median GC density was 33% lower in glaucoma patients than in healthy subjects over all tested locations. GC density was significantly reduced in glaucoma patients compared to that in healthy controls in the inferior retinal hemifield ($P < 0.001$, Table 2). Figure 4 shows the fundus image of a glaucoma patient with a paracentral scotoma in the superior visual field and corresponding reduced RNFL thickness and GC density in the inferior retina.

There was no statistically significant difference in cone density between glaucoma patients and healthy controls in either retinal hemifield (superior: $P = 0.48$, inferior: $P = 0.69$). Median cone density was very similar between glaucoma patients and healthy controls (glaucoma patients: 7,248 cells/mm², healthy controls: 7,242 cells/mm²; Table 2). There was no statistically significant inter-location difference in cone density within each group (glaucoma: $P = 0.44$; healthy controls: $P = 0.75$).

Cone density and GC density were not significantly associated in either hemifield in the healthy or glaucomatous group (Fig 5 A, C). There was a statistically significant relationship between DLS and log estimated GC density in both retinal hemifields in glaucoma patients (superior: $R^2 = 0.59$, $P < 0.001$; inferior: $R^2 = 0.28$, $P < 0.001$, Fig 5 B, D). There was no statistically significant relationship between DLS and log cone density in either group.

Median cone:GC density ratio was 3.51:1 (IQR: 2.59:1, 6.81:1) in glaucoma patients compared to 2.35:1 (IQR: 1.83:1, 2.82:1) in healthy subjects (Table 2, Fig 5

E). Ratios were significantly higher in the glaucoma patient group, compared to those in the healthy subject group ($P < 0.01$). Cone:GC ratios were not significantly different in the superior locations (without glaucomatous defect of the corresponding inferior hemifield) between glaucoma patients and healthy subjects ($P > 0.05$, Table 2). Cone:GC density ratios showed a large range in healthy controls (Fig 5 E). In view of this, attempting to calculate the true baseline GC density from *in vivo* measurements of cone density from healthy controls would be imprecise. The coefficient of variation was 30% for cone:GC ratio and 33% for GC density.

Separation of cone:GC ratio and GC density to diagnose glaucoma

Figure 6 illustrates the ROC curve for GC and cone density and cone:GC ratio. AUROC was 0.79 (95% confidence interval [CI] 0.71-0.86, $P < 0.001$) for both GC density and cone:GC ratio. Specificity was set to 80% and 90% and sensitivity was then derived. At a specificity of 80%, sensitivity was 62% for GC density (with cut-off value of 2,425 GCs/mm²) and 59% for cone:GC ratio (with cut-off values of 3.04:1). At a set specificity of 90%, sensitivity was 44% for GC density (1,935 GCs/mm²) and 49% for cone:GC ratio (3.59:1).

Ganglion cell layer thickness

GCL thickness was reduced in glaucoma patients compared to healthy controls in the area corresponding to visual field defects. The greatest GCL thickness loss across all of our patients was in the inferior retina (corresponding to superior hemifield on visual field). Median GCL thickness at test locations in glaucoma patients was 23 μ m, significantly thinner than that in healthy controls (31 μ m, $P < 0.001$, Table 2). No correlation was found between cone density and GCL thickness at any location in

either group (Spearman's ρ 0.02, $P = 0.81$). There was a significant linear relationship between DLS and GCL thickness ($R^2 = 0.52$, $P < 0.001$).

Discussion

The findings of this study lend support to the notion that although GC density is significantly reduced in glaucoma patients relative to that in healthy controls, cone density is not. The ratio of cones and overlying GCs is therefore increased in our participants with glaucoma. One of the aims of this study was determine the utility of cone imaging in the calculation of baseline GC density for more efficient identification of GC loss. The moderately large range of cone:GC density ratios in healthy controls (Fig 5 E) leads us to conclude that any prediction of baseline GC density from objective measures of cone density would be imprecise and offer little superiority over conventional methods in the identification of early glaucomatous loss.

Despite finding no statistically significant difference in cone density overall in the glaucoma patients recruited to the current study, it was still considered possible that by combining information on local cone and GC density in each patient may offer advantages over and above density alone for the identification of glaucomatous retinal damage. However, we did not find a statistically significant relationship between cone and GC density in patients or controls. Furthermore, the qualitative and quantitative (AUROC) similarity in the ROC curves for cone:GC ratio and GC density alone, further demonstrates that there is little advantage in combining cone and GC density estimates in each patient.

This is the first study to compare estimates of cone density, derived from *in vivo* images of the photoreceptor mosaic captured with an Heidelberg Retina Angiograph 2 (HRA2) without adaptive optics (AO), and psychophysical estimates of ganglion cell density and function in corresponding regions. The retinal cone density agreed

reasonably well with previously published studies using histological data^{17, 18}, AO imaging¹⁹⁻²¹ and imaging with a modified first-generation Heidelberg Retina Tomograph⁹.

Although glaucoma is a degenerative optic neuropathy affecting ganglion cells and their axons, previous studies investigating the involvement of the outer retina, including photoreceptors, in the disease have yielded somewhat conflicting results. Structural²⁻⁵ changes of the outer retina in glaucoma have been reported by some histological and clinical studies but not by others.^{6, 7} Studies involving tests of colour vision and electrophysiology have reported reduced function, suggestive of outer retinal layer abnormalities in glaucoma.²²⁻²⁷ Vincent *et al* have shown a dysfunction of cone photoreceptors in the central 24° visual field in advanced glaucoma using multifocal electroretinogram.²⁷ Cone densities presented in our study were not significantly different between glaucoma patients with visual field loss ranging from mild to moderate and age-similar healthy controls. We have included predominantly glaucoma patients with paracentral defects (within 10° of fixation) but did not find cone loss at 8.8° in glaucoma. Choi and colleagues found evidence of cone loss in glaucoma using AO imaging.² A shortening of the cone outer segments was seen with AO in areas corresponding to reduced visual sensitivity. The authors concluded that this may explain dark patches observed in AO *en face* retinal images. This is in line with a study conducted by Werner *et al* on outer retinal changes in glaucomatous and non-glaucomatous optic neuropathies observing that cones were less reflective in corresponding areas of visual field defect, resulting in dark regions in the *en face* AO images and accompanying disruptions in the outer retinal layers.⁵ Although number of cones did not differ between areas of normal and depressed visual sensitivity among glaucoma patients, and also between healthy subjects and glaucoma patients in our study, we have seen dark areas where cones could not be resolved in a number of

patients. For example, they can be observed in the inferior retina corresponding to a dense superior hemifield defect in a 47 year-old glaucoma patient (Fig 7 as supplemental data).

In this study, median cone density at 8.8° (2.42 mm) retinal eccentricity was 7,248 cells/mm² in glaucoma patients and 7,242 cells/mm² in healthy controls . These cone density estimates are somewhat lower than those reported in some histological studies (e.g. Curcio *et al*¹⁷) or from some *in vivo* studies using AO imaging devices.¹⁹⁻²¹ Curcio *et al* reported cone counts of approximately 9700 cones/mm² at ~ 2.5 mm retinal eccentricity in 8 eyes of 7 healthy, adult human donors (age 27-44 years).¹⁷ An AO imaging study conducted by Song and colleagues found a cone density of approximately 8600 cells/mm² at ~ 2.6 mm retinal eccentricity in healthy participants aged 22-65 years.²¹ Wolsely *et al* used a modified HRT to image cones in 2 healthy subjects and found a cone density of 7000 cones/mm² at ~ 2.3 mm eccentricity (extrapolated from values presented) and compares well to our data.⁹ However, Jonas *et al* reported a lower cone density of 6000 cones/mm² at only 1.5 mm (~ 5°) retinal eccentricity in 21 normal human donor eyes with a mean age of 47 ± 22 years (range 2–90 years).¹⁸ Inter-study variations in the age and refractive error of participants, in addition to possible eccentricity changes as a result of flat-mounting in histological studies, may partially account for any differences in cone density reported in the literature with those in this study. Another potential source of variability influencing reported cone densities relate to the factor used for the conversion of millimetres to degrees on the retina, along with nuances in the analysis methods applied to generate cone counts. The algorithm used for automated cone counting in this study was, however, based on work previously reported for cone images with AO devices.^{16,20} These reports found a good agreement between automated and manual counting analysis methods.

Limitations of our study must be discussed. First, as this was an exploratory study, only a small number of participants was included. Second, while we did not adjust for GC displacement relative to their corresponding photoreceptors, the displacement of GCs decreases with eccentricity and is reported to be negligible (2.34 mm) for cones at 2.42 mm (8.8°) eccentricity using the equation $y = 1.29 \times [\chi + 0.046]^{0.67}$ (y = GC eccentricity; χ = cone eccentricity) from Sjöstrand et al.²⁸ Third, some images (11 of 80 glaucoma and 5 of 75 normal) were excluded from analysis where cones could not be identified, either owing to optical limitations (e.g. poor tear film, higher astigmatism or unsteady fixation) or some, as yet, unknown change in the retina (e.g. refractive index changes).

In conclusion, our results did not show any notable advantage in using cone:GC ratios over GC density alone for identifying glaucoma. Cone:GC density ratios and GC densities show a relatively large range even in healthy controls and no relationship was found between cone and GC density in either group. On this basis, we conclude that measurements of cone density are unlikely to be helpful in the estimation of local baseline GC density in a first-time patient.

REFERENCES

1. Curcio CA, Allen KA. Topography of ganglion cells in human retina. *J Comp Neurol* 1990;300:5-25.
2. Choi SS, Zawadzki RJ, Lim MC, et al. Evidence of outer retinal changes in glaucoma patients as revealed by ultrahigh-resolution in vivo retinal imaging. *Br J Ophthalmol* 2011;95:131-41.
3. Nork TM, Ver Hoeve JN, Poulsen GL, et al. Swelling and loss of photoreceptors in chronic human and experimental glaucomas. *Arch Ophthalmol* 2000;118:235-45.
4. Panda S, Jonas JB. Decreased photoreceptor count in human eyes with secondary angle-closure glaucoma. *Invest Ophthalmol Vis Sci* 1992;33:2532-6.
5. Werner JS, Keltner JL, Zawadzki RJ, Choi SS. Outer retinal abnormalities associated with inner retinal pathology in nonglaucomatous and glaucomatous optic neuropathies. *Eye (Lond)* 2011;25:279-89.
6. Kendell KR, Quigley HA, Kerrigan LA, et al. Primary open-angle glaucoma is not associated with photoreceptor loss. *Invest Ophthalmol Vis Sci* 1995;36:200-5.
7. Wygnanski T, Desatnik H, Quigley HA, Glovinsky Y. Comparison of ganglion cell loss and cone loss in experimental glaucoma. *Am J Ophthalmol* 1995;120:184-9.
8. Kozak I. Retinal imaging using adaptive optics technology. *Saudi J Ophthalmol* 2014;28:117-22.
9. Wolsley CJ, Saunders KJ, Silvestri G, Anderson RS. Comparing mfERGs with estimates of cone density from in vivo imaging of the photoreceptor mosaic using a modified Heidelberg retina tomograph. *Vision Res* 2010;50:1462-8.
10. Thibos LN, Cheney FE, Walsh DJ. Retinal limits to the detection and resolution of gratings. *J Opt Soc Am A* 1987;4:1524-9.
11. Greaney MJ, Hoffman DC, Garway-Heath DF, et al. Comparison of optic nerve imaging methods to distinguish normal eyes from those with glaucoma. *Invest Ophthalmol Vis Sci* 2002;43:140-5.

12. Anderson RS, Evans DW, Thibos LN. Effect of window size on detection acuity and resolution acuity for sinusoidal gratings in central and peripheral vision. *J Opt Soc Am A Opt Image Sci Vis* 1996;13:697-706.
13. Thibos LN, Bradley A. New methods for discriminating neural and optical losses of vision. *Optom Vis Sci* 1993;70:279-87.
14. Drasdo N, Fowler CW. Non-linear projection of the retinal image in a wide-angle schematic eye. *Br J Ophthalmol* 1974;58:709-14.
15. Bridgeman B. Durations of Stimuli Displayed on Video Display Terminals: $(n - 1)/f +$ Persistence. *Psychol Sci* 1998;9:232-3.
16. Li KY, Roorda A. Automated identification of cone photoreceptors in adaptive optics retinal images. *J Opt Soc Am A Opt Image Sci Vis* 2007;24:1358-63.
17. Curcio CA, Sloan KR, Kalina RE, Hendrickson AE. Human photoreceptor topography. *J Comp Neurol* 1990;292:497-523.
18. Jonas JB, Schneider U, Naumann GO. Count and density of human retinal photoreceptors. *Graefes Arch Clin Exp Ophthalmol* 1992;230:505-10.
19. Chui TY, Song H, Burns SA. Individual variations in human cone photoreceptor packing density: variations with refractive error. *Invest Ophthalmol Vis Sci* 2008;49:4679-87.
20. Muthiah MN, Gias C, Chen FK, et al. Cone photoreceptor definition on adaptive optics retinal imaging. *Br J Ophthalmol* 2014;98:1073-9.
21. Song H, Chui TY, Zhong Z, et al. Variation of cone photoreceptor packing density with retinal eccentricity and age. *Invest Ophthalmol Vis Sci* 2011;52:7376-84.
22. Fazio DT, Heckenlively JR, Martin DA, Christensen RE. The electroretinogram in advanced open-angle glaucoma. *Doc Ophthalmol* 1986;63:45-54.
23. Holopigian K, Seiple W, Mayron C, et al. Electrophysiological and psychophysical flicker sensitivity in patients with primary open-angle glaucoma and ocular hypertension. *Invest Ophthalmol Vis Sci* 1990;31:1863-8.

24. Odom JV, Feghali JG, Jin JC, Weinstein GW. Visual function deficits in glaucoma. Electroretinogram pattern and luminance nonlinearities. Arch Ophthalmol 1990;108:222-7.
25. Poinoosawmy D, Nagasubramanian S, Gloster J. Colour vision in patients with chronic simple glaucoma and ocular hypertension. Br J Ophthalmol 1980;64:852-7.
26. Vaegan, Graham SL, Goldberg I, et al. Flash and pattern electroretinogram changes with optic atrophy and glaucoma. Exp Eye Res 1995;60:697-706.
27. Vincent A, Shetty R, Devi SA, et al. Functional involvement of cone photoreceptors in advanced glaucoma: a multifocal electroretinogram study. Doc Ophthalmol 2010;121:21-7.
28. Sjostrand J, Popovic Z, Conradi N, Marshall J. Morphometric study of the displacement of retinal ganglion cells subserving cones within the human fovea. Graefes Arch Clin Exp Ophthalmol 1999;237:1014-23.

FIGURE LEGENDS

Figure 1. Schematic view of a Modified Heidelberg Retina Angiograph 2 (HRA2).

A and B – Small-angle principle of a modified HRA2. Standard 30° (top) and modified small-angle 3° principle (bottom). *In vivo* cone imaging was performed at 4 retinal locations at approximately 8.8° retinal eccentricity.

C and D – Small-angle retinal scan with a scan angle of 3° (cropped to ~2.89° x 2.89°, 740 x 740 pixels) of a 58 year-old healthy control and superimposed onto fundus image.

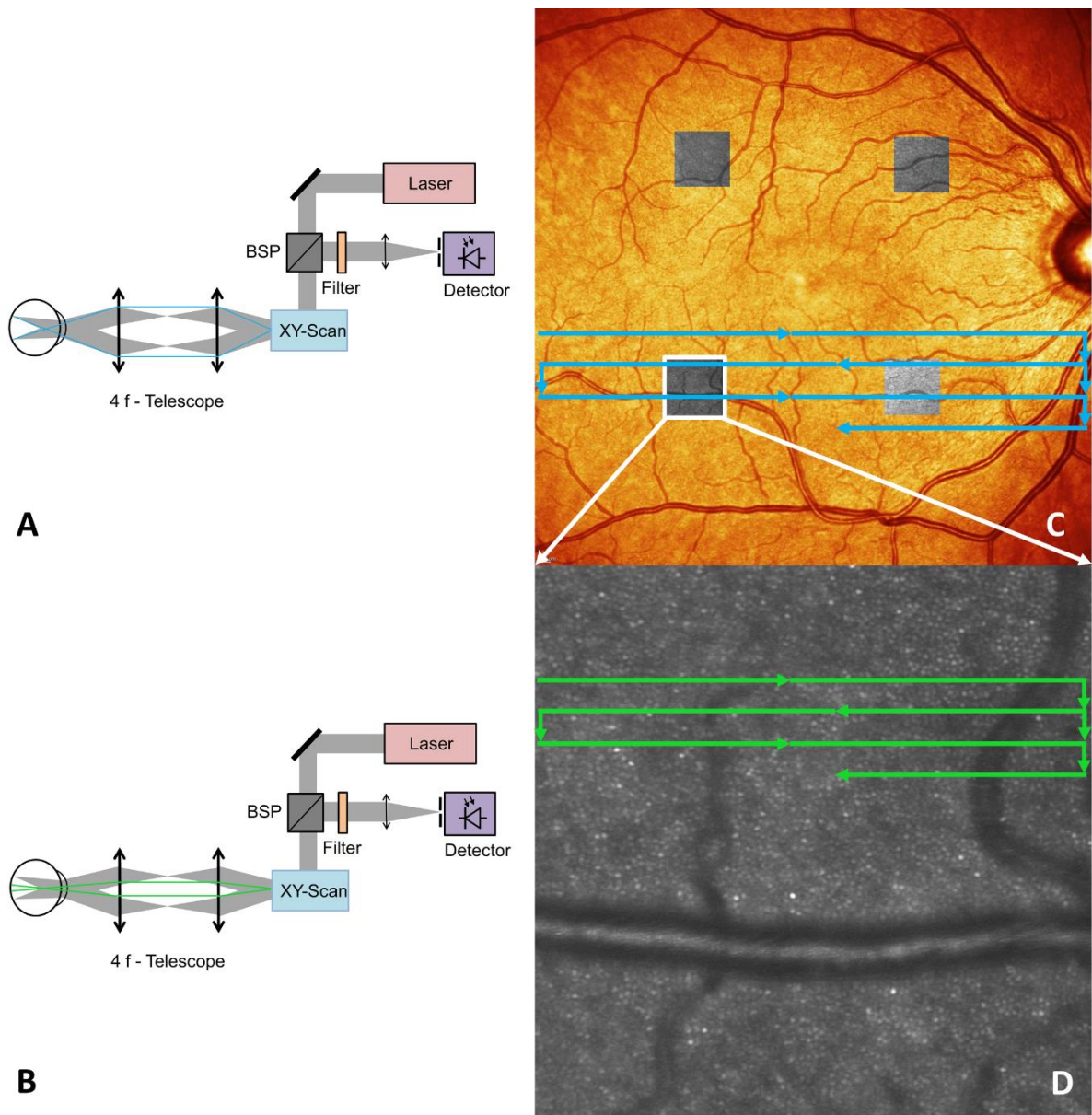


Figure 2. Examples of cone scans.

Worst (A), typical (B) and best quality (C) images of the retinal cone mosaic (D – automated cone count; note few cones were counted in blood vessels). All images were cropped to 740 x 740 pixels.

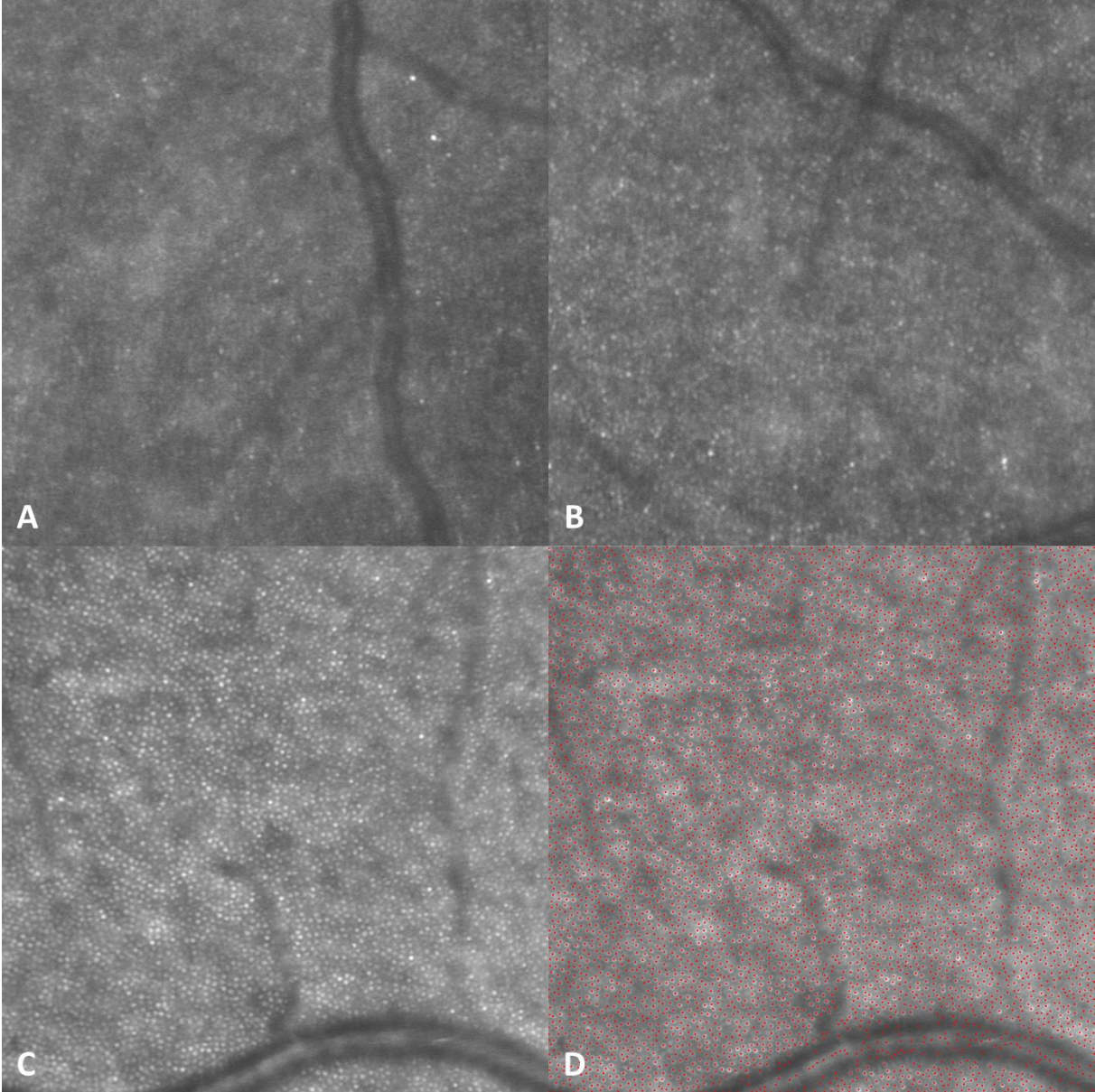


Figure 3. Adjustment of ganglion cell layer thickness measurement.

A – False-color thickness map displays thickness measurement of ganglion cell layer (GCL).

B – The posterior pole grid was subsequently adjusted such that the external border of the grid was parallel with the edge of the fundus image and the overlay transparency adjusted to visualize landmarks (e.g. blood vessels).

C – The grid was then moved to coincide with the position as of the cone image(s) captured (**D**) to produce GCL thickness values in the retinal regions examined.

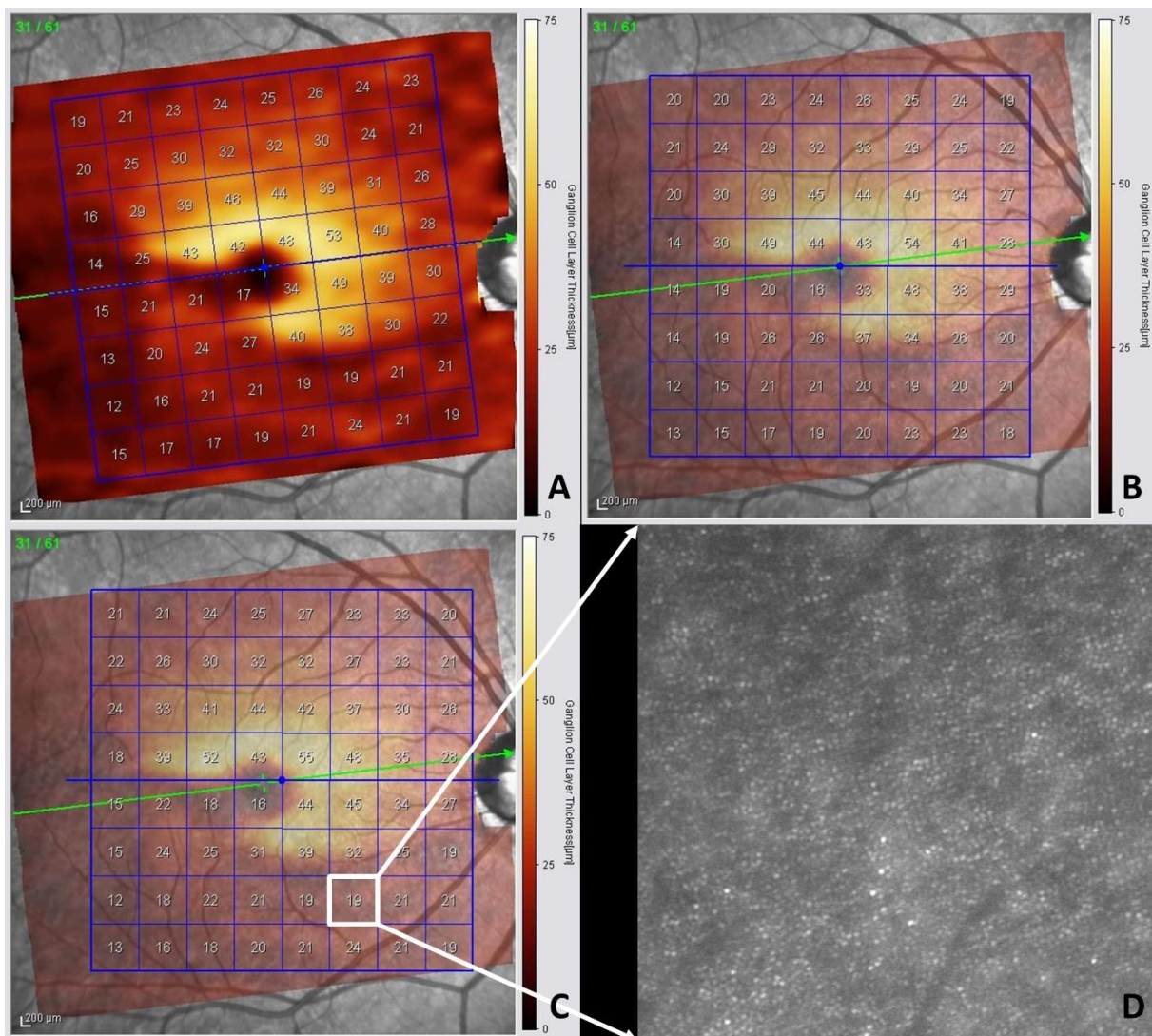


Figure 4. Fundus of a 60 year-old female patient with normal tension glaucoma. Inferior ganglion cell (GC) loss and corresponding superior field defect (pattern deviation plot). Reduced GC density and respective increased cone:GC ratio in the inferior retina.

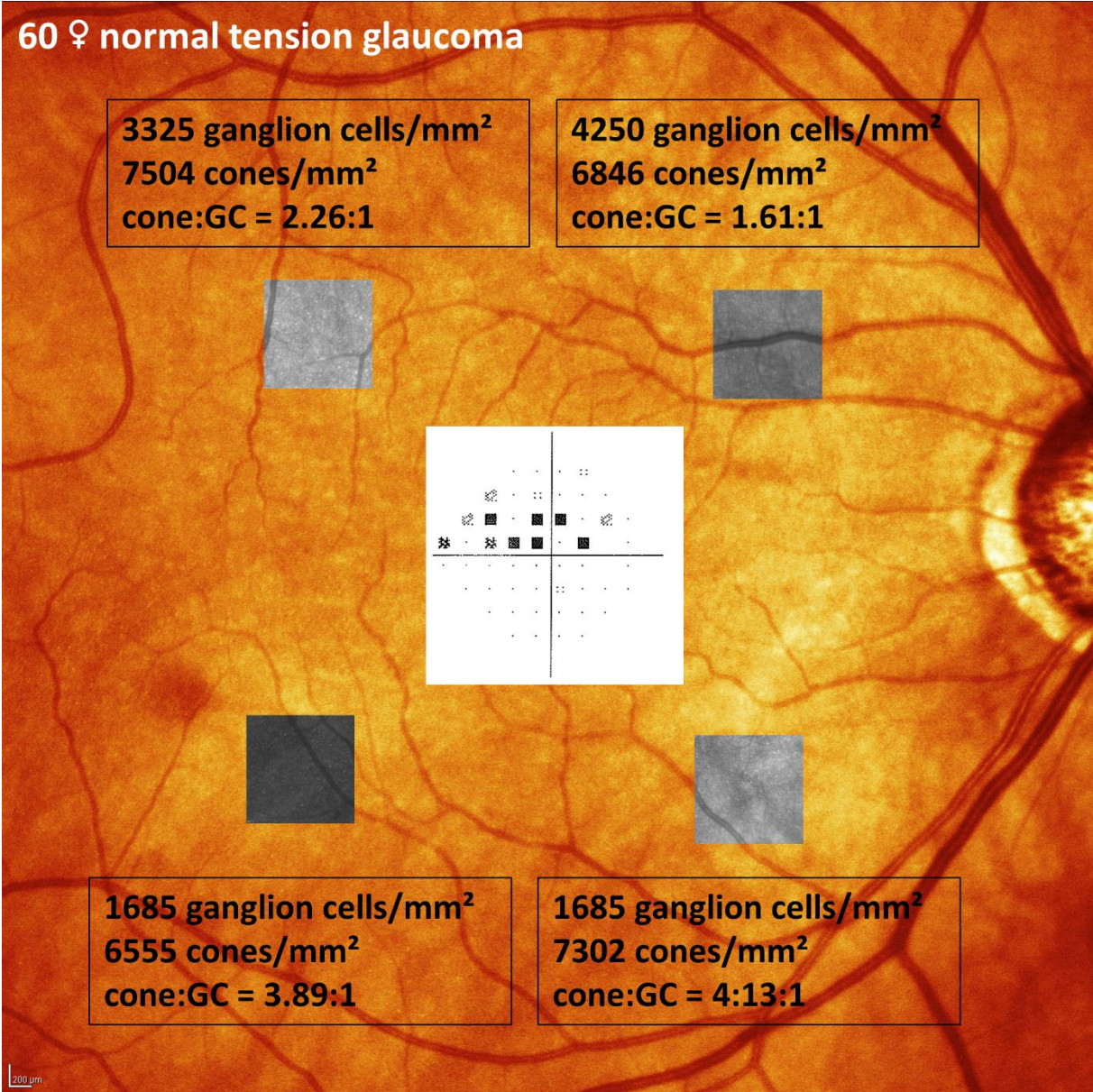


Figure 5. Relationships between local cone density, ganglion cell (GC) density and differential light sensitivity (DLS).

A, C – Relationship between local cone and GC density in the superior (A) and inferior (C) retinal hemifields of glaucoma patients and controls

B, D – Relationship between local cell (cone and GC) density and differential light sensitivity (DLS) in glaucoma patients and controls. Boxes indicate the 95% confidence intervals for cell density (height) and DLS (width) in healthy controls.

E – Range of cone:GC ratios in glaucoma patients and healthy controls.

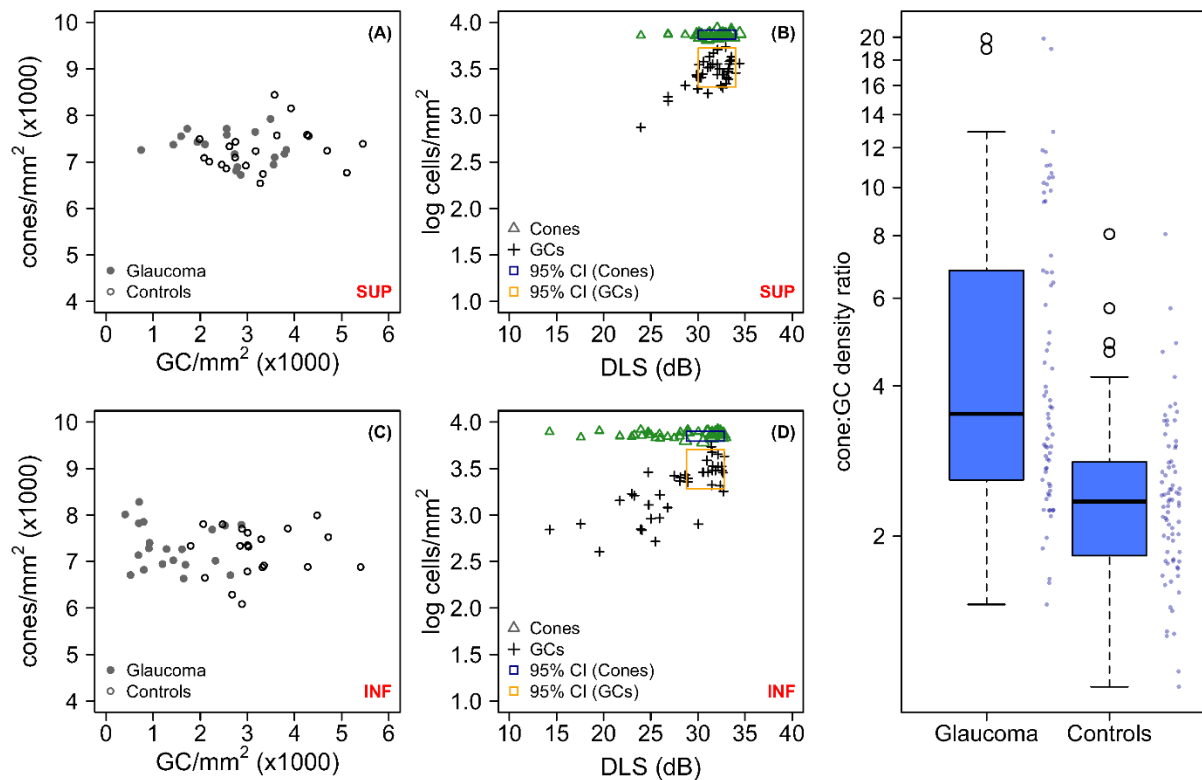


Figure 6. Receiver operating characteristic (ROC) curve for separation of ganglion cell (GC) and cone density, and cone:GC ratio to detect glaucoma.

Area under the ROC curve (AUROC) was 0.79 (95% confidence interval [CI] 0.71-0.86) for both GC density and cone:GC ratio. Sixty-nine locations of glaucoma patients were included and compared to 75 locations of healthy controls.

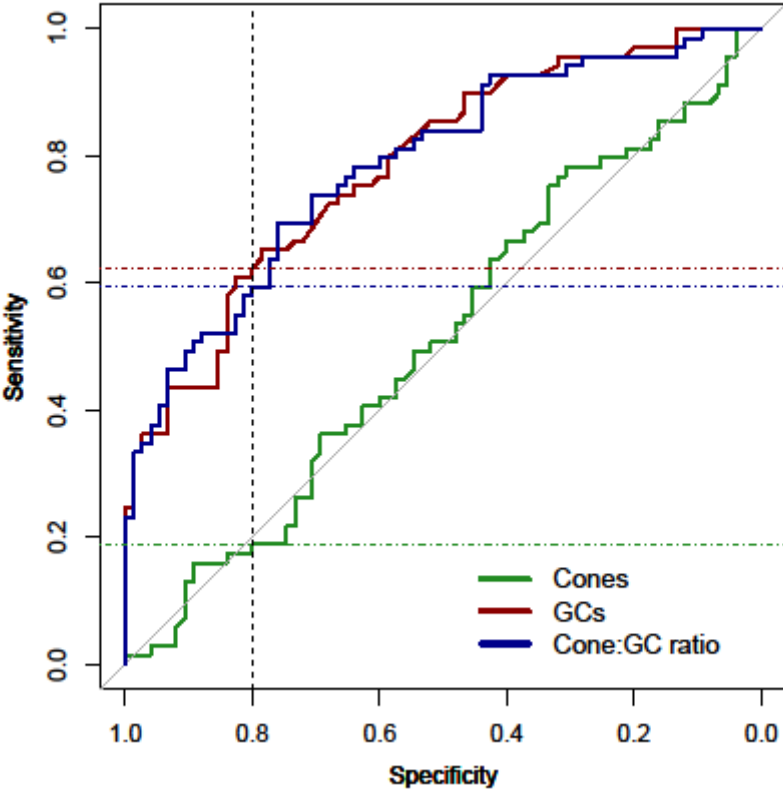


Figure 7. Example of a 47 year-old female patient with normal-tension glaucoma.

A – A large area of inferior ganglion cell (GC) loss and corresponding dense superior field defect (pattern deviation plot) are evident (nerve fibre bundle defect marked with black lines).

B – Raw cone images for all 4 locations (cropped to $\sim 2.89^\circ \times 2.89^\circ$, 740 x 740 pixels). Note blurred scans in the inferior retina with advanced retinal nerve fiber and ganglion cell loss (black arrows show dark patches where cones cannot be resolved).

Figure 7. Example of a 47 year-old female patient with normal-tension glaucoma.
A – A large area of inferior ganglion cell (GC) loss and corresponding dense superior field defect (pattern deviation plot) are evident (nerve fibre bundle defect marked with black lines).
B – Raw cone images for all 4 locations (cropped to $\sim 2.89^\circ \times 2.89^\circ$, 740 x 740 pixels). Note blurred scans in the inferior retina with advanced retinal nerve fiber and ganglion cell loss (black arrows show dark patches where cones cannot be resolved).

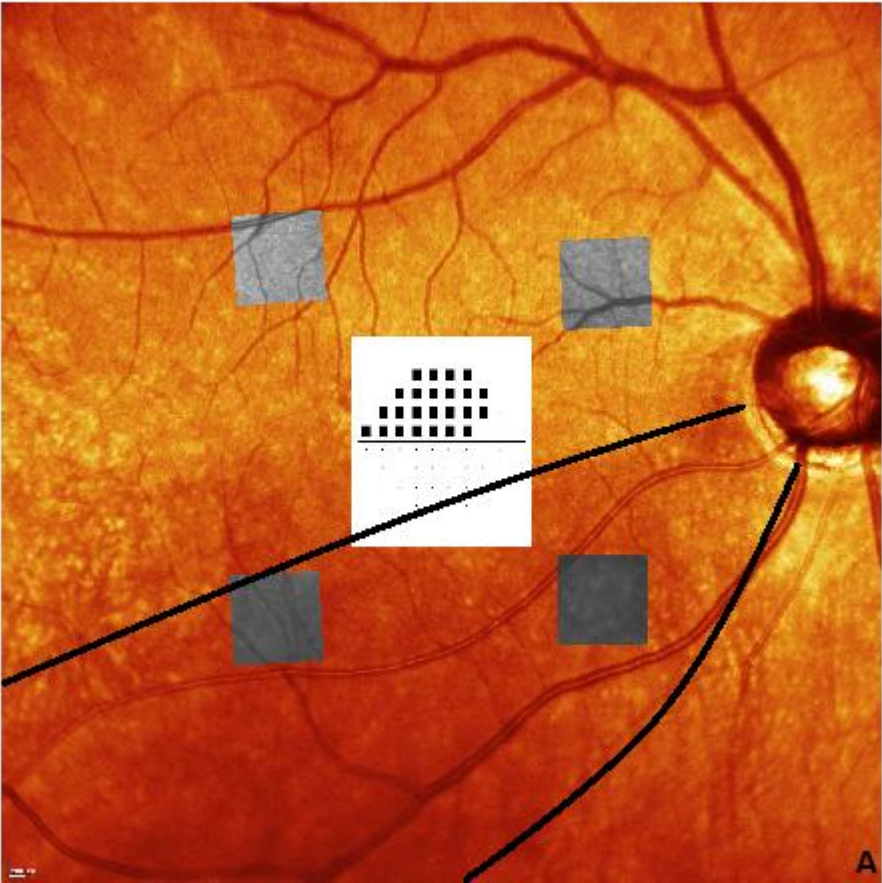


Table 1. Demographic Data of Glaucoma Patients and Healthy Participants

	Healthy	Glaucoma	<i>P</i> value
n of eyes/participants	20/20	20/20	
Age, years	57.00 [51.25, 63.75]	54.00 [50.25, 59.75]	0.58
Sex			0.74
male	6 (30)	8 (40)	
female	14 (70)	12 (60)	
Eye			1.00
right	16 (80)	15 (75)	
left	4 (20)	5 (25)	
BCVA, Snellen			0.06
6/5	20 (100)	15 (75)	
6/6	0 (0)	4 (20)	
6/9	0 (0)	1 (5)	
Spherical error, DS	+0.50 [-1.25, +0.94]	+0.13 [-1.38, +0.94]	0.68
Astigmatism, DC	-0.25 [-0.50, +0.00]	-0.75 [-1.00, -0.50]	0.003
IOP, mmHg	14.5 [13.3, 16.0]	13.0 [11.0, 15.0]	0.07
RNFL thickness, μ m	98.0 [92.0, 102.0]	68.5 [57.8, 78.0]	<0.001

Data are absolute values (%), median [interquartile range] as appropriate.

Abbreviations: *BCVA* best-corrected visual acuity, *DC* dioptre cylinder, *DS* dioptre sphere, *IOP* intraocular pressure, *MD* mean defect, *n* number of eyes/participants, *PSD* pattern standard deviation, *RNFL* retinal nerve fiber layer.

Table 2. Cone Density, estimated GC Density and Cone:GC Ratio, GCL Thickness and Visual Sensitivity at different retinal locations

	Healthy	Glaucoma	<i>P</i> value
GCs/mm²			
superior nasal	3023 [2550, 3713]	2483 [1995, 3119]	0.06
inferior nasal	2885 [2200, 3314]	971 [727, 2099]	<0.001
superior temporal	3325 [2441, 4301]	2684 [2262, 3166]	0.09
inferior temporal	3373 [2670, 4034]	1458 [727, 2252]	<0.001
All locations	3158 [2503, 4060]	2125 [971, 2763]	<0.001
Cones/mm²			
superior nasal	7295 [6845, 7763]	7196 [6972, 7499]	0.91
inferior nasal	7213 [6842, 7777]	7332 [7082, 7965]	0.32
superior temporal	7098 [6996, 7352]	7238 [6968, 7685]	0.55
inferior temporal	7432 [6814, 7630]	7215 [6700, 7495]	0.39
All locations	7242 [6876, 7700]	7248 [6968, 7634]	0.79
Cone:GC ratio			
superior nasal	2.43:1 [1.78:1, 2.76:1]	2.94:1 [2.25:1, 4.44:1]	0.08
inferior nasal	2.48:1 [2.15:1, 3.34:1]	6.76:1 [3.73:1, 10.78:1]	<0.001
superior temporal	2.13:1 [1.72:1, 2.02:1]	2.73:1 [2.22:1, 3.60:1]	0.07
inferior temporal	2.18:1 [1.81:1, 2.56:1]	5.24:1 [3.01:1, 10.45:1]	<0.001
All locations	2.35:1 [1.83:1, 2.82:1]	3.51:1 [2.59:1, 6.81:1]	<0.001
GCL thickness, μm			
superior nasal	31.0 [30.0, 33.0]	27.5 [22.0, 32.8]	0.08
inferior nasal	30.0 [29.0, 32.0]	21.0 [19.0, 23.5]	<0.001
superior temporal	32.0 [29.0, 34.0]	29.0 [24.0, 32.0]	0.06
inferior temporal	32.5 [28.8, 35.0]	20.0 [17.0, 23.0]	<0.001
All locations	30.8 [29.1, 33.3]	23.3 [21.0, 27.5]	<0.001
Visual sensitivity, dB†			
superior nasal	32.7 [31.3, 33.2]	29.9 [28.6, 32.5]	0.005
inferior nasal	32.1 [31.3, 32.8]	24.5 [17.2, 27.5]	<0.001
superior temporal	32.4 [31.5, 33.1]	31.3 [30.1, 32.8]	0.03
inferior temporal	31.8 [31.1, 32.1]	25.3 [20.5, 28.7]	<0.001
All locations	32.1 [31.4, 32.9]	28.6 [24.4, 30.9]	<0.001

Data are median [interquartile range] retinal locations at ~ 8.8° eccentricity.

Abbreviations: GC ganglion cell, GCL ganglion cell layer, *n* number of locations,.

Note: Not all of the 4 locations for each glaucoma patient or healthy participant could be imaged with some locations therefore excluded. The majority of images (> 80%, 75 images included/80 total number of locations in healthy subjects and 69/80 in glaucoma patients) were, however, analyzed. In **bold**, significantly reduced GC density and visual field sensitivity, and increased cone:GC ratio mainly in the inferior retina. Cone count remains constant over all locations. Most of the glaucoma patients (90%) had glaucomatous defects in the superior hemifield.